

Current transport in a superconducting superlattice system

Bor-Luen Huang and Chung-Yu Mou

Department of Physics, National Tsing Hua University, Hsinchu 30043, Taiwan

Abstract

We investigate the effect of the superlattice structure on the single particle transport along the c -axis of high temperature superconductors. In particular, superlattice systems that consists of metals/insulators and d -wave superconductors (NS/IS superlattice) are considered. We find that for the NS superlattice in the large mass anisotropy limit of the metal, the density of state in the low energy section is bulk d -wave like except that the position of the quasi-particle peak can be considerably smaller than the gap value, while for the IS superlattice, the quasi-particle peak remains at the gap value. We also calculate the nonlinear differential conductance in the planar junction measurement. It is found that the width of the Andreev peak at zero-bias may be affected strongly by the superlattice structure, specifically, it can be considerably reduced due to the destructive interference of the Andreev reflections from all the superconductors. Such a reduction in the width makes the Andreev peak resonant-like and has been observed in a recent experiment.

PACS numbers: 74.20.-z, 74.50.+r, 74.80.-g, 74.25.Fy

I. INTRODUCTION

The artificial prepared superlattices have been an important system for investigating the relevancy of periodic structure to the physical properties of the bulk system. The idea is that if the dephasing length of the electron extends over many periods, the superlattice structure becomes relevant. Therefore, by engineering the periodic structure appropriately, one is able to tune the effective parameters that electrons experience, thus it may enable us to access more regions in the parameter space. In particular, one may be able to engineer the density of state so that the transport properties can be changed. Such systems have motivated a lot of studies both experimentally and theoretically [1]. There are many outstanding issues arising from the investigation of superlattice systems. For instance, the giant magnetoresistance (MR) observed in magnetic superlattices, such as Fe/Cr, has triggered serious investigation of the transport through heterostructure of metal and ferromagnetic materials [2].

The superlattice that has superconductors involved is another important system. It was shown in an early study that certain superlattice structure can close the energy gap of s-wave superconductors [3], which is interesting by itself and may have real applications in the future. The interest in superlattices with superconductors has been further boosted up since the discovery of the high temperature superconductors (HTSC) [4]. The layered structure along the c-axis and particularly the existence of closely packed CuO_2 planes makes HTSC a natural-occurring superconducting superlattice system. A great body of work has thus been devoted to investigate the c-axis dynamic properties during the past [5]. After the intense work for so many years, it now becomes clear that in the overdoped region, the normal state of high Tc superconductors is metallic like for both c-axis and in-plane directions [6]. In particular, the splitting due to hopping between adjacent CuO_2 planes in a unit cell are seen directly in recent photoemission experiments [7]. While these works imply that single particle hopping definitely occurs along the c direction, it is not clear how exactly one should model the transport properties of the high Tc cuprates along the c-axis in the superconducting phase and how the superlattice structure affects the single particle

transportation along the c direction.

The splitting observed in the photoemission experiments implies that neighboring CuO_2 planes in a unit cell are strongly coupled by a large hopping integral. Therefore, one can model it by a single superconducting layer, which is coupled to the superconducting layers in adjacent unit cells via an effective hopping integral t_{eff} . This is also consistent with the fact that the coherence length along the c direction is about the width of each superconducting layer. The problem is then how one should model layers between adjacent superconducting layers. It was pointed in Ref. [8] that there exist two distinct limits, depending on the ratio t_{eff} to T_c . In the limit when t_{eff} is much smaller than T_c , the system behaves more like a NSNSN ...NSN (or a ISISISISI) superlattice, i.e., a normal metal-superconductor (NS) or insulator-superconductor (IS) superlattice. On the other hand, if t_{eff} is close to T_c in magnitude, different unit cells are coupled strongly and the system behaves as a usual anisotropic superconductor. In this work, we shall be mainly investigating the nonlinear transport in the limit when t_{eff} is much smaller than T_c . In order to model the c-axis transport in HTSC, we shall consider several concrete models, for instance, the NS and IS superlattice models as both of them can give rise metallic behaviors in c and ab directions in the normal state. Another possible modification is to consider a NS superlattice with a large mass anisotropy (effective mass in the c-axis \ll effective mass in ab directions) in the metal so that electrons essentially hop along the c-axis in the NS superlattice model. Two quantities will be calculated: (1) the density of state for single particles, which will be useful for the transport measurement with high resistance contact. (2) the differential conductance (dI/dV) for measurements with low resistance contact, such as measurement made by planar junctions. We shall include the d-wave nature and consider general Fermi surface topology. Our results will be useful for artificial superlattices such as the $YBa_2Cu_3O_{7-\delta}/PrBa_2Cu_3O_{7-\delta}$ superlattice system [4]. At phenomenological level, they also provide insights to the issue that to what extent the c-axis of HTCS can be thought as a NS superlattice or a IS superlattice, in particular, how the superlattice structure along the c-axis affects the tunneling spectrum. Our results indicate that in the case for a NS superlattice, if the mass anisotropy is small,

the superlattice structure will induce subgap structure in the density of state. For large mass anisotropy in the metal, however, the bulk d-wave-like density of state is reproduced with the quasi-particle peak shifted to a smaller value, in contrast to the case when we model the c-axis as a IS superlattice where the quasi-particle peak remains at the gap value. The NS superlattice model provides a possible explanation of why some measurements of the gap size along the c direction give smaller values [4,9]. We also calculate the dI/dV curve for measurements using planar junction or point contact with large contact area along the c-direction. Two important features are found to be due to the superlattice structure: (1) The width of the Andreev peak at zero bias is considerably smaller than the gap due to destructive interference of Andreev reflections from all the superconductors. This gives a natural explanation to why in some old measurement, the Andreev peak along the c-axis appeared to be so sharp and was thought as zero-bias resonant conductance peak [10]. (2) There exist distinct oscillations in the region when V is larger than the gap size. This is also a result of interference from all in the interfaces. In particular, the IS superlattice will provide a rising background so that these oscillations gradually rises as V increases. Both features are observed in a recent measurement of Au/Bi2212 junctions near T_c [11].

This paper is organized as follows: In Sec.II, the density of state is calculated in the framework of Bogolubov de-Genne equation. We show that in the large mass anisotropy limit of the NS superlattice, the usual d-wave like behavior is reproduced. We also calculate the case when it is a SI superlattice and briefly compare these results. In Sec.III, the non-linear dI/dV curve for planar junctions is calculated and its relation to experiments is discussed. Finally, we give a concluding remark in Sec.IV.

II. THEORETICAL FORMULATION AND DENSITY OF STATE

We shall start by investigating the density of state for a NS superlattice. A NS superlattice with a spherical Fermi surface and s-wave for superconductors was previously considered by Hahn [3] to model transport along the c-axis for YBCO. To account for the c-axis trans-

port of high Tc cuprates, we shall extend it to include d-wave nature and use a more general Fermi surface. In particular, during our calculation, we shall also briefly address the effect due to a particular form for the c-axis hopping $t_c = -t_\perp \cos^2(2\phi)$. This particular form of hopping is suggested from the measurement of angle-resolved photoemission (ARPES) and band theoretical calculation [7,12]. Here ϕ is the angle $\tan^{-1}(q_y/q_x)$ (see Fig.1).

We shall first calculate the density of state. In the most general case, the density of state is given by

$$n(E) = \int \int \int \frac{dq_x dq_y d\kappa}{(2\pi)^3} \delta(E - E(q_x, q_y, \kappa)), \quad (1)$$

when κ is the Bloch wavenumber along the c-axis. For given E , q_x , and q_y , if $\kappa(E, q_x, q_y)$ can be found, $n(E)$ can be rewritten as

$$n(E) = \int \int \frac{dq_x dq_y}{(2\pi)^3} n_1(E), \quad (2)$$

where we have defined the one dimensional density of state by $n_1(E) \equiv \left| \frac{\partial \kappa}{\partial E} \right|$. In this case, one needs to find $\kappa(E, q_x, q_y)$. For a NS superlattice, a suitable framework for calculating $\kappa(E, q_x, q_y)$ is the Bogolubov de-Genne equation which can be written as

$$\begin{bmatrix} \hat{h} & \Delta \\ \Delta^* & -\hat{h} \end{bmatrix} \begin{bmatrix} u(\mathbf{r}) \\ v(\mathbf{r}) \end{bmatrix} = E \begin{bmatrix} u(\mathbf{r}) \\ v(\mathbf{r}) \end{bmatrix}, \quad (3)$$

where $\hat{h} = \xi_q - \mu_F$, $\Delta = \Delta_0 \cos(2\phi)$ in the superconducting part while in the metal part, we simply set $\Delta_0 = 0$. We shall assume a general form for ξ_q

$$\begin{aligned} \xi_q &= \frac{\hbar^2}{2m'}(q_x^2 + q_y^2) + \frac{\hbar^2}{2m_S} q_z^2 && \text{in the superconductor,} \\ &= \frac{\hbar^2}{2m}(q_x^2 + q_y^2) + \frac{\hbar^2}{2m_N} q_z^2 && \text{in the metal.} \end{aligned}$$

Since the system is translationally invariant in x and y directions, q_x and q_y are conserved so that we can write $u(\mathbf{r}) = u(z) \exp^{i(q_x x + q_y y)}$ and $v(\mathbf{r}) = v(z) \exp^{i(q_x x + q_y y)}$. Eqs.(3) then reduces to one dimensional equations. In the metal part, $\Delta_0 = 0$, q_x and q_y are on the Fermi surface so that we may parameterize $q_x = k_F \sin \theta \cos \phi$ and

$q_y = k_F \sin \theta \sin \phi$, where $k_F \equiv \sqrt{\frac{2m\mu_F}{\hbar^2}}$ and θ is the azimuthal angle along the c direction. In this parameterization, for a given energy E , the particle (+) and hole (-) momentum become $p^\pm = \sqrt{\frac{2m_S}{\hbar^2} [\mu_F(1 - \frac{m}{m'} \sin^2 \theta) \pm \sqrt{E^2 - \Delta^2}]}$ in the superconducting part, while $k^\pm = \sqrt{\frac{2m_N}{\hbar^2} (\mu_F \cos^2 \theta \pm E)}$ in the metal. Furthermore, Eq.(2) becomes

$$n(E) = \int \int \frac{k_F^2 \sin \theta \cos \theta d\phi d\theta}{(2\pi)^3} \frac{\partial \kappa}{\partial E}. \quad (4)$$

It is important to note that the factor $1 - m/m' \sin^2 \theta$ has to be positive as it represents $(p^\pm)^2$ at the Fermi surface in the absence of Δ . Therefore, *large m/m' , i.e., large mass anisotropy in the metal, restricts electrons to hop only along the c -axis.*

The wavefunctions $u(z)$ and $v(z)$ have to be continuous at boundaries. Since the system is periodic, it is sufficient to impose the boundary conditions within a unit cell (see Fig. 1)

$$\begin{aligned} u_N(0) &= u_S(0), v_N(0) = v_S(0) \\ u'_N(0) &= u'_S(0), v'_N(0) = v'_S(0) \\ u_S(b) &= \lambda u_N(-a), v_S(b) = \lambda v_N(-a) \\ u'_S(b) &= \lambda u'_N(-a), v'_S(b) = \lambda v'_N(-a) \end{aligned} \quad (5)$$

where the last two equations follow from the Bloch theorem with $|\lambda| = 1$. Following Ref. [13] and using the above boundary conditions, one finds that λ satisfies

$$D_0 + D_1\lambda + D_2\lambda^2 + D_3\lambda^3 + D_4\lambda^4 = 0 \quad (6)$$

where D_0, D_1, \dots, D_4 are all real. Since $|\lambda| = 1$, the four roots to Eq.(6) are in the form $\exp^{\pm(i\theta_1)}$ and $\exp^{\pm(i\theta_2)}$. This implies that $D_0 = D_4, D_1 = D_3$. Thus the solutions to Eq.(6) is completely determined by the ratio $\frac{D_1}{D_0}$ and $\frac{D_2}{D_0}$.

$$\cos(\kappa d) = \frac{1}{4} \left[-\frac{D_1}{D_0} \pm \sqrt{\left(\frac{D_1}{D_0}\right)^2 - 4\frac{D_2}{D_0} + 8} \right], \quad (7)$$

where we have expressed λ by $\exp(i\kappa d)$ with $d = a + b$. We shall see that the positive sign is for the particle excitation, while the negative sign is for the hole excitation. It is

convenient to measure the length by $\xi_N \equiv \hbar^2 k_F / \sqrt{m m_N \Delta_0}$ and energy by Δ_0 ($\varepsilon \equiv E / \Delta_0$). Denoting $A \equiv a / \xi_N$, $B \equiv b / \xi_N$ and $\varepsilon_F \equiv \mu_F / \Delta_0$, after some algebra and using the Andreev approximation [13], we find that for a fixed ϕ and θ

$$\frac{D_1}{D_0} = -4 [\cos(2\varepsilon_F A X) \cos(2\varepsilon_F \gamma B X_m) \Gamma_1 - \sin(2\varepsilon_F A X) \sin(2\varepsilon_F \gamma B X_m) \Gamma_2], \quad (8)$$

$$\begin{aligned} \frac{D_2}{D_0} = & 4\Gamma_2^2 + (g^2 - 1) [1 + \cos(4\varepsilon_F A X) + \cos(4\varepsilon_F \gamma B X_m) - 2\Gamma_3] \\ & + (g^2 + 1) \cos(4\varepsilon_F A X) \cos(4\varepsilon_F \gamma B X_m) - 2g \sin(4\varepsilon_F A X) \sin(4\varepsilon_F \gamma B X_m). \end{aligned} \quad (9)$$

Here $X = \cos \theta$, $\gamma = \sqrt{m_S / m_N}$, $X_m = \sqrt{1 - (m / m') \sin^2 \theta}$ and $g \equiv (\cos \theta / \gamma X_m + \gamma X_m / \cos \theta) / 2$. For $\varepsilon^2 > \cos^2 2\phi$, Γ_i are given by

$$\Gamma_1 = \cos\left(\frac{\varepsilon A}{X}\right) \cos\left(\frac{\varepsilon_\phi B}{X_m}\right) - g \frac{\varepsilon}{\varepsilon_\phi} \sin\left(\frac{\varepsilon A}{X}\right) \sin\left(\frac{\varepsilon_\phi B}{X_m}\right), \quad (10)$$

$$\Gamma_2 = g \cos\left(\frac{\varepsilon A}{X}\right) \cos\left(\frac{\varepsilon_\phi B}{X_m}\right) - \frac{\varepsilon}{\varepsilon_\phi} \sin\left(\frac{\varepsilon A}{X}\right) \sin\left(\frac{\varepsilon_\phi B}{X_m}\right), \quad (11)$$

$$\Gamma_3 = \cos^2\left(\frac{\varepsilon_\phi B}{X_m}\right) [1 + \cos(4\varepsilon_F A X)] + \cos^2\left(\frac{\varepsilon A}{X}\right) [1 + \cos(4\varepsilon_F \gamma B X_m)], \quad (12)$$

where $\varepsilon_\phi = \sqrt{\varepsilon^2 - \cos^2 2\phi}$; while for $\varepsilon^2 < \cos^2 2\phi$, one simply replaces $\cos(\sin)$ by \cosh (\sinh), and ε_ϕ by $\sqrt{\cos^2 2\phi - \varepsilon^2}$.

Homogenous case This is the case when $m = m'$ and $m_N = m_S$. Therefore, $g = 1$. We have $\Gamma_1 = \Gamma_2 \equiv \Gamma(\varepsilon)$, as a result, we find that $\cos(\kappa d) = \Gamma \cos[2\varepsilon_F (A + B)X] \pm \sqrt{1 - \Gamma^2} \sin[2\varepsilon_F (A + B)X]$, recovering results obtained in Ref. [13] with $\frac{k^+ + k^-}{2}$ and $\frac{p^+ + p^-}{2}$ being approximated by $2\varepsilon_F (A + B)X$. It is instructive to check the case of $\Delta_0 = 0$. In this case, we have $p^\pm = k^\pm$ and thus $\Gamma = 1$. We find that $\kappa = k^\pm$. Therefore, \pm represents particle and hole channels respectively. For the homogeneous case, since $\Gamma^2 \leq 1$, we may write $\Gamma = \sin \alpha(\varepsilon)$. It is then easy to see that $n_1(\varepsilon) = \frac{1}{d} \left| \pm \frac{\partial \alpha}{\partial \varepsilon} \right|$ are the same for particles and holes. As shown in Fig. 2(a), if we use negative ε to represent the hole, the one dimensional density of state is an even function of ε . Fig. 2(b) shows the result when $m_S \neq m_N$, it is seen that there is no particle-hole symmetry any more. Note that the values of A and B are chosen to be close the data for YBCO: $\xi_N \approx \xi_{ab} \approx 1.5nm$, $a \approx 0.85nm$, and $b \approx 0.38nm$. It is also instructive to check that the NS superlattice model also includes the limit when

t_{eff} is close to T_c in magnitude as one can simply set $A = 0$, $B = 1$ in the homogeneous case. In this case, Γ is simply $\cosh \sqrt{\varepsilon^2 - \cos^2 2\phi}$ for $\varepsilon^2 \geq \cos^2 2\phi$ and $\cos \sqrt{\cos^2 2\phi - \varepsilon^2}$ for $\varepsilon^2 < \cos^2 2\phi$. Thus $n_1(\varepsilon) = \frac{1}{d} \frac{\varepsilon}{\sqrt{\varepsilon^2 - \cos^2 2\phi}}$ for $\varepsilon^2 \geq \cos^2 2\phi$, which reproduces the usual d-wave density of state after integration over ϕ , see Fig.3(a).

Fig. 3(b) shows a case when A becomes nonzero. It is obvious that the introduction of any small N section (i.e., small A) moves the quasi-particle peak into the subgap region while leaving in a peak-like structure at $E = \Delta_0$. Fig. 3(c) shows a more realistic case for $A = 0.57$ and $B = 0.21$ (homogeneous). The structure at $E = \Delta_0$ becomes too small to be observed.

Large mass anisotropy limit We now discuss the effect of increasing the ratio m/m' . A possible candidate to describe the high T_c cuprates is the limit when m/m' becomes so large that electrons essentially can only hop along the c-axis between CuO_2 planes in different unit cells. As we pointed it out already that large m/m' restricts θ to be small. For infinite m/m' , we can simply set $X = \cos \theta = 1$ and perform the following reduced integral

$$n_r(E) = \int \frac{k_F^2 d\phi}{(2\pi)^3} \frac{\partial \kappa}{\partial E} \Big|_{X=1}. \quad (13)$$

If the superconducting part is s-wave, $n_r(E)$ is $\frac{k_F^2}{(2\pi)^2} \frac{\partial \kappa}{\partial E} \Big|_{X=1}$. Consider the case when $m_S = m_N$, it is easy to see that $X_\theta = g = 1$. We find that $\Gamma_1 = \Gamma_2 \equiv \Gamma(\varepsilon)$ and $\cos(\kappa \pm 2\varepsilon_F(A + B)X)d = \Gamma(\varepsilon)$. The point is that the one dimensional density of state $\partial \kappa / \partial \varepsilon$ starts from a gap whose size is determined by the root to $\Gamma(\varepsilon_0) = 1$ for $\varepsilon_0 \leq 1$. Near ε_0^+ , one has

$$\left| \frac{\partial \kappa}{\partial \varepsilon} \right| = \frac{1}{d} \frac{1}{\sqrt{1 - \Gamma^2}} \left| \frac{\partial \Gamma}{\partial \varepsilon} \right| \approx \frac{1}{d} \sqrt{\frac{\Gamma'(\varepsilon_0)}{2}} \frac{1}{\sqrt{\varepsilon - \varepsilon_0}}, \quad (14)$$

which has a BCS-like square root singularity but at smaller energy ($\varepsilon_0 < 1$). Therefore, in the lower energy section, we obtain a bulk s-wave like density of state with quasi-particle peak at smaller energy. For high energy sections, near the zone boundary of κ , the BCS-like square root singularity will repeat again. For d-wave superconductors, Eq.(13) is replaced by

$$\left| \frac{\partial \kappa}{\partial \varepsilon} \right| = \frac{1}{d} \frac{1}{\sqrt{1 - \Gamma^2}} \left| \frac{\partial \Gamma}{\partial \varepsilon} \right| \approx \sqrt{\frac{\Gamma'(\varepsilon_0)}{2}} \frac{|\cos 2\phi|}{\sqrt{|\varepsilon - \varepsilon_0| |\cos 2\phi|}}, \quad (15)$$

where ε_0 depends on ϕ . Thus, the BCS-like square root singularity is preserved for a fixed ϕ . In Fig.4, we show the result of direct integration over ϕ for different m_S/m_N ratios. It is clear that at low energy section, $n_r(E)$ behaves similar to the bulk d-wave density of state, except that the quasi-particle peak moves to smaller energy. If we take $\Delta_0 \approx 30 - 40$ meV, the quasi-particle peak is around 8 - 11 meV which is close to what experiments have seen [4]. Note that another difference between the above results and the true bulk d-wave density of state may lie at high energy section. In general, the superlattice structure introduces coupling among the wavevector of the electron and the reciprocal lattice vectors of the superlattice, i.e., $(0, 0, 2n\pi/d)$ ($\equiv \mathbf{Q}$). The coupling strength depends on the magnitude of the Fourier component $\Delta_0(\mathbf{Q})$. If the superlattice periodicity is good, $\Delta_0(\mathbf{Q})$ will not be small. The superlattice structure will force $n_r(E)$ to have similar d-wave like structure whenever the zone boundary ($\cos \kappa d = \pm 1$) is encountered in high energy sectors. However, if the system is not large enough along the c direction or the dephasing length of the electron is short, one may expect that $\Delta_0(\mathbf{Q})$ is small and hence the repeated structure in high energy section will not appear.

We now address the effect due to the anisotropy of the c-axis hopping. In particular, we consider $t_c = -t_\perp \cos^2(2\phi)$. As it is clear from the above calculations and also the following calculation for the IS superlattice, the density of state depends only on the ratio of m_S to m_N (defined as γ^2). Obviously, if both the intra-superconducting cells and inter-superconducting cells c-axis hoppings follow the same form. There will be no effect at all. However, new features may arise if they do not follow the same form. In particular, we find that if either m_S or m_N does not depend on ϕ , a second peak could arise inside the subgap region. In views of past experimental findings, this seems to be unlikely. Therefore, we shall not consider such possibility in the following.

IS superlattice As a comparison, we now consider the case when the materials between CuO₂ planes in different unit cells are modeled by insulators. For this purpose, we introduce a large potential V to every metal cell so that the metal cells effectively become insulators. We shall consider the simplest case when $m = m' = m_N = m_S$. When the superconducting

gap vanishes, this model reduces to the standard Kronig-Penny, therefore, it represents a natural generalization of NIN superlattice. In this case, k^\pm becomes purely imaginary. Following the same procedure, we find that Eqs. (8) and (9) are essentially the same except that g is now defined by $i(\alpha + 1/\alpha)/2$ with $\alpha = \sqrt{\mu_F \cos^2 \theta / (V - \mu_F \cos^2 \theta)}$ and $\cos(2\varepsilon_F AX)$ and $\sin(2\varepsilon_F AX)$ being replaced by $\cosh(2\varepsilon_F AX/\alpha)$ and $\sinh(2\varepsilon_F AX/\alpha)$. The new Γ_i are given by (for $\varepsilon^2 > \cos^2 2\phi$)

$$\Gamma_1 = \cosh\left(\frac{\varepsilon A \alpha}{X}\right) \cos\left(\frac{\varepsilon_\phi B}{X}\right) + ig \frac{\varepsilon}{\varepsilon_\phi} \sinh\left(\frac{\varepsilon A \alpha}{X}\right) \sin\left(\frac{\varepsilon_\phi B}{X}\right), \quad (16)$$

$$\Gamma_2 = -ig \cosh\left(\frac{\varepsilon A \alpha}{X}\right) \cos\left(\frac{\varepsilon_\phi B}{X}\right) - \frac{\varepsilon}{\varepsilon_\phi} \sinh\left(\frac{\varepsilon A \alpha}{X}\right) \sin\left(\frac{\varepsilon_\phi B}{X}\right), \quad (17)$$

$$\Gamma_3 = \cos^2\left(\frac{\varepsilon_\phi B}{X}\right) \left[1 + \cosh\left(\frac{4\varepsilon_F AX}{\alpha}\right)\right] + \cosh^2\left(\frac{\varepsilon A \alpha}{X}\right) [1 + \cos(4\varepsilon_F BX)], \quad (18)$$

while again for $\varepsilon^2 < \cos^2 2\phi$, one replaces $\cos(\sin)$ by $\cosh(\sinh)$, and ε_ϕ by $\sqrt{\cos^2 2\phi - \varepsilon^2}$. In Fig.5, we show a typical result for the three dimensional density of state for the SI superlattice. Because for energy below the gap, $\varepsilon^2 < \cos^2 2\phi$, quasi particles and quasi holes are both evanescent, the quasi-particle peaks now move to the gap value (except that there is a slight asymmetry in particles and holes). Technically, this is due to that for $\varepsilon^2 < \cos^2 2\phi$, all factors in Γ_i are not oscillatory and thus the right hand side in Eq.(7) is greater than one, without any propagating solutions. This is similar to the case for a bulk d-wave superconductor as we analyzed for Fig.3(a), so one gets quasi-particle peaks right at the gap value.

The dramatic difference in the positions of the quasi-particle peaks for the NS and IS superlattices offers a useful check on both models. For artificial made NS superlattices, the reduction in the position of the quasi-particle peak has been observed in Ref. [4]. However, for the c-axis measurements on real high Tc materials, the results are controversial and remains to be clarified in the future [14].

III. NONLINEAR DIFFERENTIAL CONDUCTANCE

We now investigate the differential conductance (dI/dV) for the measurement with low resistance contact, such as measurements made by planar junctions or by point contact with large contact area. The schematic setup is shown in Fig.6. In principle, at first and last interfaces that connect with the electrodes, there may exist insulating layers. This will be included as interfacial scattering potentials. The most important feature coming out from this type of measurement, in comparison to the high contact resistance measurement, is the possible exhibition of the excess current due to the Andreev reflection (AR). However, for a long time, the AR along the c direction was not observed until quite recently Andreev peaks with reduced widths are observed in Au/Bi2212 junctions near T_c [11].

In this section, we shall carry out a theoretical calculation of the dI/dV curves based on the NS/IS superlattice models. We shall show that the width of the Andreev peak in such systems is often reduced due to the superlattice structure. A similar problem in which the superconductor in each cell is replaced by another metal (N') was analyzed in Ref. [15] using a full quantum mechanic approach. Here we shall approximate the voltages in each layer (either in N or S) by constants such that the slope of the voltage, thus the electric field, is fixed. This is exact in the superconducting cell, however, in the metal cell the approximation is valid only if the electric field is weak (specifically, eVa/nd has to be smaller than ε_F). To obtain the differential conductance, we need to match the quasi-particle wave functions at boundaries: $z = nd$ and $z = nd + b$. At the boundary $z = nd$, the quasi-particle wave function for the normal metal is

$$\begin{aligned} \psi(z = nd) \equiv \begin{pmatrix} u(z = nd) \\ v(z = nd) \end{pmatrix} = A_n \begin{pmatrix} 1 \\ 0 \end{pmatrix} e^{ik_n^+ nD} + B_n \begin{pmatrix} 1 \\ 0 \end{pmatrix} e^{-ik_n^+ nD} \\ + C_n \begin{pmatrix} 0 \\ 1 \end{pmatrix} e^{ik_n^- nD} + D_n \begin{pmatrix} 0 \\ 1 \end{pmatrix} e^{-ik_n^- nD}, \end{aligned} \quad (19)$$

where we have measured energy in unit of Δ_0 and lengths by ξ_N , hence $D = d/\xi_N$ and $k_n^\pm = \sqrt{\cos^2 \theta + (\pm\varepsilon - V_n^N)/\varepsilon_F}$ with $V_n^N = \frac{V}{\Delta_0}(1 - n/N_0)$ and N_0 being the total number of

layers. For the superconducting region at the right hand side of $z = nd$, the wavefunction is

$$\begin{aligned} \phi(z = nd) = & E_{n+1} \begin{pmatrix} u_0 \\ v_0 \end{pmatrix} e^{ip_{n+1}^+ nD} + F_{n+1} \begin{pmatrix} u_0 \\ v_0 \end{pmatrix} e^{-ip_{n+1}^+ nD} \\ & + G_{n+1} \begin{pmatrix} v_0 \\ u_0 \end{pmatrix} e^{ip_{n+1}^- nD} + H_{n+1} \begin{pmatrix} v_0 \\ u_0 \end{pmatrix} e^{-ip_{n+1}^- nD}. \end{aligned} \quad (20)$$

Here the wavevector p_{n+1}^\pm is measured by k_F and is given by $\sqrt{\gamma_1(1 - \gamma_2 \sin^2 \theta) + \gamma_1/\varepsilon_F(\pm\varepsilon_\phi - V_{n+1}^S)}$ with $\gamma_1 \equiv \frac{m_S}{m_N}$ and $\gamma_2 \equiv \frac{m}{m'}$, $V_{n+1}^S = \frac{V}{\Delta_0}[1 - (nD + B)/N_0D]$ (measured by k_F), and the coherent factors $u_0^2 = (1 + \varepsilon_\phi/\varepsilon)/2$ and $v_0^2 = (1 - \varepsilon_\phi/\varepsilon)/2$. The boundary conditions at $z = nd$ are

$$\psi(nd) = \phi(nd),$$

$$\frac{m_N}{m_S} \frac{\partial}{\partial z} \phi(nd) - \frac{\partial}{\partial z} \psi(nd) = \frac{2m_N H}{\hbar^2} \phi(nd), \quad (21)$$

where we have introduced a delta potential with strength H at this interface [16]. This provides a relation between A_n, B_n, C_n, D_n and $E_{n+1}, F_{n+1}, G_{n+1}, H_{n+1}$, which is conveniently expressed by introducing a transfer matrix M_1

$$M_1 \begin{pmatrix} E_{n+1} \\ F_{n+1} \\ G_{n+1} \\ H_{n+1} \end{pmatrix} = \begin{pmatrix} A_n \\ B_n \\ C_n \\ D_n \end{pmatrix}. \quad (22)$$

Here the full expression of M_1 is given by

$$\begin{pmatrix} \frac{u_0}{2} [1 + i\frac{2Z}{k_n^+} + \frac{p_{n+1}^+}{\gamma_1 k_n^+}] e^{i2\varepsilon_F [p_{n+1}^+ - k_n^+] nD} & \frac{u_0}{2} [1 + i\frac{2Z}{k_n^+} - \frac{p_{n+1}^+}{\gamma_1 k_n^+}] e^{-i2\varepsilon_F [p_{n+1}^+ + k_n^+] nD} \\ \frac{u_0}{2} [1 - i\frac{2Z}{k_n^+} - \frac{p_{n+1}^+}{\gamma_1 k_n^+}] e^{i2\varepsilon_F [p_{n+1}^+ + k_n^+] nD} & \frac{u_0}{2} [1 - i\frac{2Z}{k_n^+} + \frac{p_{n+1}^+}{\gamma_1 k_n^+}] e^{-i2\varepsilon_F [p_{n+1}^+ - k_n^+] nD} \\ \frac{v_0}{2} [1 + i\frac{2Z}{k_n^-} + \frac{p_{n+1}^-}{\gamma_1 k_n^-}] e^{i2\varepsilon_F [p_{n+1}^- - k_n^-] nD} & \frac{v_0}{2} [1 + i\frac{2Z}{k_n^-} - \frac{p_{n+1}^-}{\gamma_1 k_n^-}] e^{-i2\varepsilon_F [p_{n+1}^- + k_n^-] nD} \\ \frac{v_0}{2} [1 - i\frac{2Z}{k_n^-} - \frac{p_{n+1}^-}{\gamma_1 k_n^-}] e^{i2\varepsilon_F [p_{n+1}^- + k_n^-] nD} & \frac{v_0}{2} [1 - i\frac{2Z}{k_n^-} + \frac{p_{n+1}^-}{\gamma_1 k_n^-}] e^{-i2\varepsilon_F [p_{n+1}^- - k_n^-] nD} \end{pmatrix}$$

$$\left. \begin{aligned} & \frac{v_0}{2} \left[1 + i \frac{2Z}{k_n^+} + \frac{p_{n+1}^-}{\gamma_1 k_n^+} \right] e^{i2\epsilon_F [p_{n+1}^- - k_n^+] nD} & \frac{v_0}{2} \left[1 + i \frac{2Z}{k_n^+} - \frac{p_{n+1}^-}{\gamma_1 k_n^+} \right] e^{-i2\epsilon_F [p_{n+1}^- + k_n^+] nD} \\ & \frac{v_0}{2} \left[1 - i \frac{2Z}{k_n^+} - \frac{p_{n+1}^-}{\gamma_1 k_n^+} \right] e^{i2\epsilon_F [p_{n+1}^- + k_n^+] nD} & \frac{v_0}{2} \left[1 - i \frac{2Z}{k_n^+} + \frac{p_{n+1}^-}{\gamma_1 k_n^+} \right] e^{-i2\epsilon_F [p_{n+1}^- - k_n^+] nD} \\ & \frac{u_0}{2} \left[1 + i \frac{2Z}{k_n^-} + \frac{p_{n+1}^-}{\gamma_1 k_n^-} \right] e^{i2\epsilon_F [p_{n+1}^- - k_n^-] nD} & \frac{u_0}{2} \left[1 + i \frac{2Z}{k_n^-} - \frac{p_{n+1}^-}{\gamma_1 k_n^-} \right] e^{-i2\epsilon_F [p_{n+1}^- + k_n^-] nD} \\ & \frac{u_0}{2} \left[1 - i \frac{2Z}{k_n^-} - \frac{p_{n+1}^-}{\gamma_1 k_n^-} \right] e^{i2\epsilon_F [p_{n+1}^- + k_n^-] nD} & \frac{u_0}{2} \left[1 - i \frac{2Z}{k_n^-} + \frac{p_{n+1}^-}{\gamma_1 k_n^-} \right] e^{-i2\epsilon_F [p_{n+1}^- - k_n^-] nD} \end{aligned} \right), \quad (23)$$

with Z ($\equiv \frac{Hm_N}{\hbar^2 k_F}$) characterizing the interface potential. Note that in principle different layers may have different Z . The above formalism is for the NS superlattice. To model a IS superlattice, one adds a large potential V to the metal cell so that k_n^\pm become evanescent and are replaced by $\sqrt{\cos^2 \theta + \frac{1}{\epsilon_F} (\pm \epsilon - V_n^N - \frac{V}{\Delta_0})}$.

Similar boundary conditions are also imposed at $z = nd + b$, and yield the relation

$$M_2 \begin{pmatrix} E_{n+1} \\ F_{n+1} \\ G_{n+1} \\ H_{n+1} \end{pmatrix} = \begin{pmatrix} A_{n+1} \\ B_{n+1} \\ C_{n+1} \\ D_{n+1} \end{pmatrix} \quad (24)$$

where M_2 can be obtained by M_1 simply by the following changes: $nD \rightarrow nD+B$, $k_n^\pm \rightarrow k_{n+1}^\pm$ and $H \rightarrow -H$. Thus the effective transfer matrix that connects the n th cell and $(n+1)$ th cell has the form

$$M_{n \rightarrow n+1} \begin{pmatrix} A_n \\ B_n \\ C_n \\ D_n \end{pmatrix} = \begin{pmatrix} A_{n+1} \\ B_{n+1} \\ C_{n+1} \\ D_{n+1} \end{pmatrix}, \quad (25)$$

where $M_{n \rightarrow n+1} = M_2 \cdot M_1^{-1}$. Note that coherence in superconducting region is assumed so that no phase memory is lost when quasi-particles tunnel from one superconducting cell to another one. The transfer matrix of the whole system for N_0 -layers, \hat{T}_{N_0} , is thus obtained by

$$\hat{T}_{N_0} = \prod_{n=0}^{N_0-1} M_{n \rightarrow n+1}, \quad (26)$$

so the coefficients in the N_0 -th cell $A_{N_0}, B_{N_0}, C_{N_0}, D_{N_0}$ are connected with those in first cell A_0, B_0, C_0, D_0 by the relation

$$\hat{T}_{N_0} \begin{pmatrix} A_0 \\ B_0 \\ C_0 \\ D_0 \end{pmatrix} = \begin{pmatrix} A_{N_0} \\ B_{N_0} \\ C_{N_0} \\ D_{N_0} \end{pmatrix}. \quad (27)$$

We shall further impose the boundary conditions near electrodes. Firstly, because electron can only flow into the system from the high voltage electrode, we require

$$A_0 = 1, D_0 = 0. \quad (28)$$

Secondly, in the low voltage electrode, we impose the condition

$$B_{N_0} = C_{N_0} = 0, \quad (29)$$

so that no particle (both hole and electron) flows into the system from the lowest voltage side. Eqs. (28) and (29) are then sufficient to determine the amplitude B_0 and C_0 in terms components of T_{N_0} , we find that

$$\begin{aligned} B_0 &= (T_{N_0}^{31} T_{N_0}^{23} - T_{N_0}^{21} T_{N_0}^{33}) / (T_{N_0}^{22} T_{N_0}^{33} - T_{N_0}^{32} T_{N_0}^{23}) \\ C_0 &= (T_{N_0}^{31} T_{N_0}^{22} - T_{N_0}^{21} T_{N_0}^{32}) / (T_{N_0}^{23} T_{N_0}^{32} - T_{N_0}^{22} T_{N_0}^{33}). \end{aligned} \quad (30)$$

To obtain the differential conductance in terms of the above coefficients, we apply the same argument used in Ref. [16] in which one treats the superlattice between electrodes as a scattering center. We obtain the same expression for the differential conductance

$$dI/dV = 2N(E_F)ev_F \mathcal{A} (1 - |B_0(eV)|^2 + |C_0(eV)|^2), \quad (31)$$

where \mathcal{A} is the area for the junction.

To illustrate the behavior of the differential conductance, it is useful to consider the simplest case when $N_0 = 1$, i.e., a NSN structure. This will be the more realistic configuration for measurement on what is often referred as the NS junction in the literature [16]. We shall

consider the case when $m = m' = m_N = m_S$ and $\varepsilon_F \gg 1$ so that one can apply the so-called Andreev approximation in which one approximates k_n^\pm and p_n^\pm by 1 ($\theta = 0$ and $n = 0$), i.e., the wavevectors along c-axis are approximated by k_F . This is the approximation used to derive the differential conductance of the NS junction in the BTK theory [16]. Nevertheless, it turns out that for a NSN junction, such approximation leads to a result with zero Andreev current. A closer examination shows that in the large ε_F , one has to keep the expansion of both k_n^\pm and p_n^\pm to the first order in $(\pm\varepsilon - V_n^N)/\varepsilon_F$ or $(\pm\varepsilon_\phi - V_{n+1}^S)/\varepsilon_F$ when computing the phase terms. We find that such manipulation leads to

$$\begin{aligned}
 B_0 &= 0 \\
 C_0 &= \frac{-1 + e^{2\varepsilon_\phi B i}}{-u_0^2 + v_0^2 e^{2\varepsilon_\phi B i}} u_0 v_0.
 \end{aligned} \tag{32}$$

Therefore, for $\varepsilon^2 < \cos^2 2\phi$, ε_ϕ is purely imaginary and hence in the limit of large B , C_0 approaches $-v_0/u_0$, recovering the standard BTK result. For $\varepsilon^2 \geq \cos^2 2\phi$, ε_ϕ is positive and C_0 oscillates with periods, determined only by B . The oscillation of C_0 was actually observed in Ref. [17]. It is a result of interference of Andreev reflection from both interfaces (left and right interfaces) of the superconductors. In Fig.7(a), we show the dI/dV curves of directional tunneling ($\phi = 0$ and without using the Andreev approximation) for different B with A being fixed at one. One sees that the period of oscillation decreases for increasing B , in consistent with the above analysis.

As N_0 exceeds one, the lengthscale A also participates in determining the oscillations. In this case, the Andreev approximation always yields $B_0 = 0$ when $Z = 0$ because $T_{N_0}^{21}$ and $T_{N_0}^{32}$ are always zero in this approximation. The total conductance is thus determined by C_0 given by $-T_{N_0}^{31}/T_{N_0}^{33}$. Fig. 7(b) shows the calculated differential conductance for the directional tunneling (electrons incident perpendicular to the interface) of a NS superlattice by using the exact expressions of the transfer matrix. As a demonstration, here we consider the homogeneous case with the total number of layers being ten. One sees that a repeated main Andreev peak is already seen around $\varepsilon \approx 4$, resembling the repeated structure when crossing the zone boundary in infinite systems. Note that these repeated structures may

not be exhibited in real experiments as the dephasing length could easily get shorter in higher voltage. Nevertheless the main Andreev peak at zero-bias will still be a special feature to superconducting superlattices. *Most importantly, unlike the width of the Andreev peak in the NS junction, the width of the Andreev peak can be much less than Δ_0 .* This is due to destructive interference of the Andreev reflections from all the superconductors. As the normal metal diminishes, the separation between these Andreev peaks increases, and eventually, only the one at the zero bias survives. At the same time, the width of the Andreev peak extend to Δ_0 . In addition to this feature, there are also small oscillations between these Andreev peaks. These oscillations are also results of the interference from all the interfaces. They have fixed period in terms of energy as demonstrated in Fig. 7(c).

It is tempting to make an analogy between the NS superlattice and the diffraction gratings (each superconductor cell seems to be analogous to a slit in the grating). However, crucial differences do exist and make the interference in the NS superlattice system more complicated: (i) The Andreev reflection from each superconductor has to pass all other superconductors in front of it to get to the electrode where the interference happens. (ii) The incident wave that arrives at each superconductor has to pass all other superconductors in front of it. As a result, a precise dependence of the separation and the width on A and B are complicated and can only be computed numerically. Nevertheless, in a special limit in which A is large and B is very small, one may disregard B in computing the phase. The result is similar to that for the diffraction grating: Because the path between successive superconducting cells is $2AV$, we have

$$|C_0|^2 \propto \left[\frac{\sin(N_0 AV)}{\sin(AV)} \right]^2. \quad (33)$$

Therefore, the positions of the main Andreev peaks are independent of the number of layers N_0 and are located at $m\pi/A$ with m being nonnegative integers. On the other hand, the minima are located at $m\pi/N_0A$ with m being nonnegative integers, and hence the width of the Andreev peak is π/N_0A . All of these results can be explicitly checked numerically. Fig. 7(d) is a simple demonstration in which the calculated dI/dV curve based on Eq.(33)

is compared with that based on the exact calculation. One sees that Eq.(33) gives excellent results in the lower energy sector. Note that for large A , the Andreev peak gets sharper and becomes more like a zero-bias resonant conductance peak. This is very different from the other limit when A goes to zero, where the Andreev peak is a plateau, extending from zero-bias to $V = \Delta_0$.

We now analyze the IS superlattice. Essentially, the dI/dV curve for the IS superlattice has a similar behavior as shown in Fig. 7(e) in which an Andreev peak sits at the zero-bias, *with reduced width*. The difference is that the small oscillations now sit in a rising background. The reason for this rising behavior is due to that when V increases, the insulators becomes more transparent so that the conductance increases. The differential conductance shown Fig.7(e) resembles a recent observed data in a underdoped BSCCO sample [11]. This resemblance suggests that a IS superlattice is more appropriate to model the c-axis transport in the underdoped regime.

IV. CONCLUSIONS AND ACKNOWLEDGMENTS

In conclusion, we have investigated the effects of the superlattice structure on the single particle transport along the c-axis of the high T_c superconductors. Based on superlattice models that consist of metals/insulators and d-wave superconductors (NS/IS superlattices), we find that a crucial difference between the NS superlattice and the IS superlattice lies in the positions of the quasi-particle peaks in the measurement of density of state. In the large mass anisotropy limit of the metal for the NS superlattice, the density of state in the low energy section is still bulk d-wave like except that the position of the quasi-particle peak is reduced considerably, while for the IS superlattice, the quasi-particle peak remains at the gap value. The width of the Andreev peak at zero-bias in the planar junction measurement is also shown to be affected strongly by the superlattice structure. It is found that this width can be considerably reduced due to the destructive interference of the Andreev reflections from all the superconductors. In addition to this feature, there are also distinct oscillations with

smaller amplitudes extending out from the main Andreev peak. Most importantly, for the IS superlattice, these oscillations sit in a rising background, in consistent with experiments.

This work is supported by the NSC of Taiwan under Grant No. NSC 89-2112-M-007-091. We thank Profs. H.H.Lin, T.M. Hong and C. S. Chu for useful discussions.

REFERENCES

- [1] E.L.Ivchenko, G.E.Pikus, Superlattices and Other Heterostructures-Symmetry and Optical Phenomena 2nd. (Springer, Germany, 1997).
- [2] See, for example, G.Oomi, Y.Uwatoko, T.Sakai, H.Fujimori, J. Magn. Magn. Mater. **156**:(1-3) 402-404 (1996); L.Lazar, J.S.Jiang, G.P.Felcher, A.Inomata, S.D.Bader, J. Magn. Magn. Mater. **223**, 299 -303 (2001).
- [3] A. Hahn, Physica **B 165&166**, 1065 (1990).
- [4] J.C. Martinez et al. con-mat/002111; M. Varela et al. Phys. Rev. Lett. **83**, 3936 (1999); Douglas H. Lowndes et al. Phys. Rev. Lett. **65**, 1160 (1990).
- [5] See. for example, K. Takenaka, et al. Phys. Rev. B **50**, 6534 (1994).
- [6] For a review, see S. L. Cooper and K. E. Gray, in *Physical Properties of High Temperature Superconductors IV*, ed. by D. M. Ginsberg (World Scientific, Singapore, 1994).
- [7] For recent progress, see Y. -D. Chuang et al. cont-mat/0107002.
- [8] L. N. Bulaevskii and R. Rammal, Phys. Rev. B **44**, 9768 (1991).
- [9] Hung-Wen Cheng, Ph.D. thesis, National Tsing Hua University (2000).
- [10] See Fig.2 in Saion Sinha and K.-W.Ng, Phys. Rev. Lett.**80**,1296 (1998).
- [11] H.S. Chang, H.J Lee, and M. Oda, cond-mat/0107354.
- [12] T. Xiang and W. N. Hardy, Phys. Rev. B **63**, 024560 (2001).
- [13] A.P. Van Gelder, Phys. Rev. **181**, 787(1969).
- [14] The reduction of the quasi-particle peak was observed in Ref. [9] for In/BSCCO system. However, for measurements on YBCO, one observed a dip at zero bias, see for example, M. Covington and L. H. Greene, Phys. Rev. B **62**, 12440 (2000).
- [15] G. S. Ning et al. Phys Rev. B **51**, 4641 (1995).

[16] G.E.Blonder, M.Tinkham, T.M.Klapwijk, Phys. Rev. B **25**, 4515 (1982).

[17] See Fig.9 in G.E.Blonder and M. Tinkham, Phys. Rev. B **27**, 112 (1983).

V. FIGURE CAPTIONS

Fig.1 The unit cell in a NS superlattice and the definition of angle ϕ . We shall denote $d = a + b$ and assume that the q_x and q_y directions are infinite.

Fig.2 (a) The one dimensional density of state for the case when $\theta = 0$, $\phi = 0$, $m = m'$ and $m_N = m_S$. Here A and B are chosen to be close the data for YBCO: $A = 0.57$, $B = 0.21$. It is seen that the density of state possess particle and hole symmetry. (b) The one dimensional density of state for the same parameters used in (a) except that now $m_S/m_N = 0.5$. The asymmetry between particles and holes are evident.

Fig.3 (a) The three dimensional density of state for the homogeneous case when $A = 0$ and $B = 1$. Here $n(\varepsilon)$ is measured by the unit $k_F^2/4\pi^2d$. (b) A similar plot for the case when $A = 0.1, 0.2$ and $B = 1$. One sees that the quasi-particle peak moves in the subgap region, leaving a peak-like structure at $\varepsilon = 1$. (c) A more realistic case when $A = 0.57$ and $B = 0.21$.

Fig.4 The three dimensional density of state in the infinite mass anisotropy limit ($m/m' \rightarrow \infty$, $A = 0.57$, and $B = 0.21$) for the low energy section. The position of the quasi-particle is considerably smaller than Δ_0 .

Fig.5 The three dimensional density of state for the SI superlattice in the simplest case when all the masses are the same and the other paramters are $A = 0.57$, and $B = 0.21$. Here $V = 1.2\varepsilon_F$ and $\varepsilon_F = 10$. One sees that the quasi-particle peak remains at $\varepsilon = 1$.

Fig.6 Schematic plot of the setup for low contact resistance measurement.

Fig.7 (a) The calculated differential conductance for a NSN junction based on Eqs.(30) and (31) for different lengths of the superconductor. Here $\phi = 0$, $\varepsilon_F = 100$, and dI/dV is measured in terms of $2N(E_F)ev_F\mathcal{A}$. (b) The dI/dV curve (integrated over ϕ) for a NS

superlattice with 10 layers. Here we assume $m = m' = m_S = m_N$, $A = 0.57$, $B = 0.21$, $Z = 0$, and $\varepsilon_F = 20$. (c) The energies of local maxima of the dI/dV versus their indices. Except a few steps in-between, the energy is linear in the index, indicating that the period of small oscillations in Fig.7(b) is a constant. The steps occurs when one jumps across the main Andreev peaks. (d) Solid line: The dI/dV curve for a NS superlattice with 15 layers for $A = 1$ and $B = 0.01$. Here we assume that $m = m' = m_S = m_N$, $Z = 0$, $\phi = 0$ and $\varepsilon_F = 20$. Dash line: A fitting based on Eq.(33) gives excellent results in low energies. (e) The differential conductance for a SI superlattice with 10 layers. The parameters used here are $A = 0.57$, $B = 0.21$, $Z = 0$, $\gamma_1 = 0.5$, $\gamma_2 = 2.87$, $\varepsilon_F = 20$, $V/\Delta_0 = 22$. This curve is close to to the dI/dV curve in low temperature recently observed in Ref. [11] (see their Fig.2(b)).

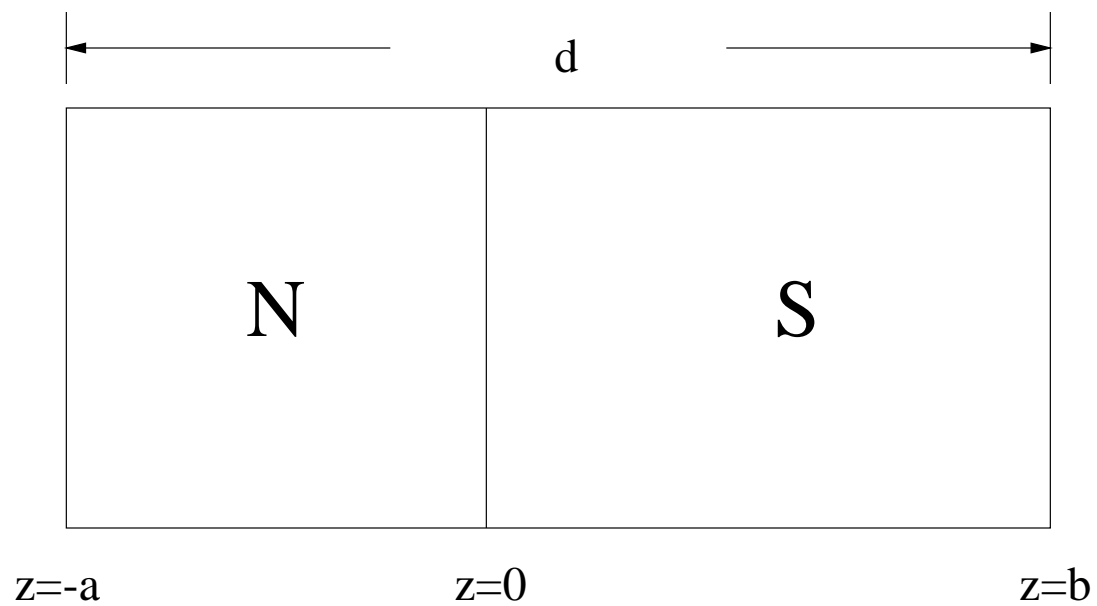
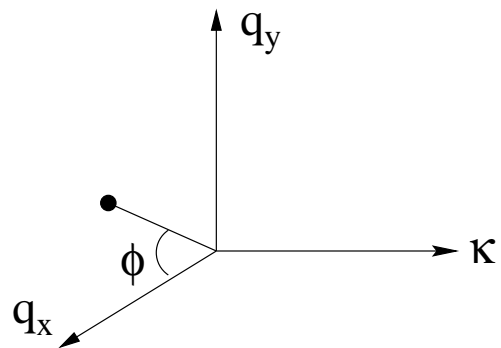


Fig. 1

Fig. 2(a)

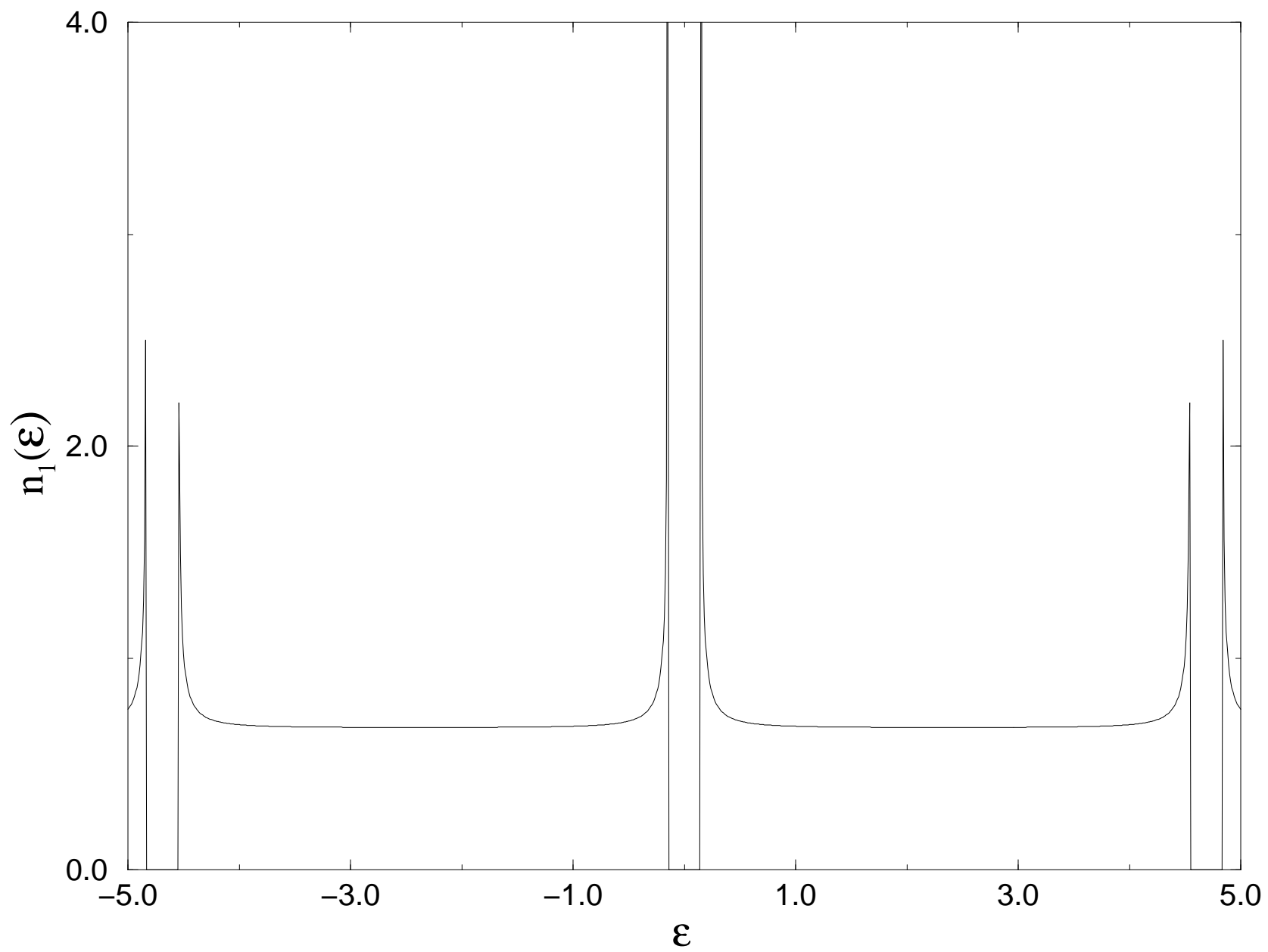


Fig. 2(b)

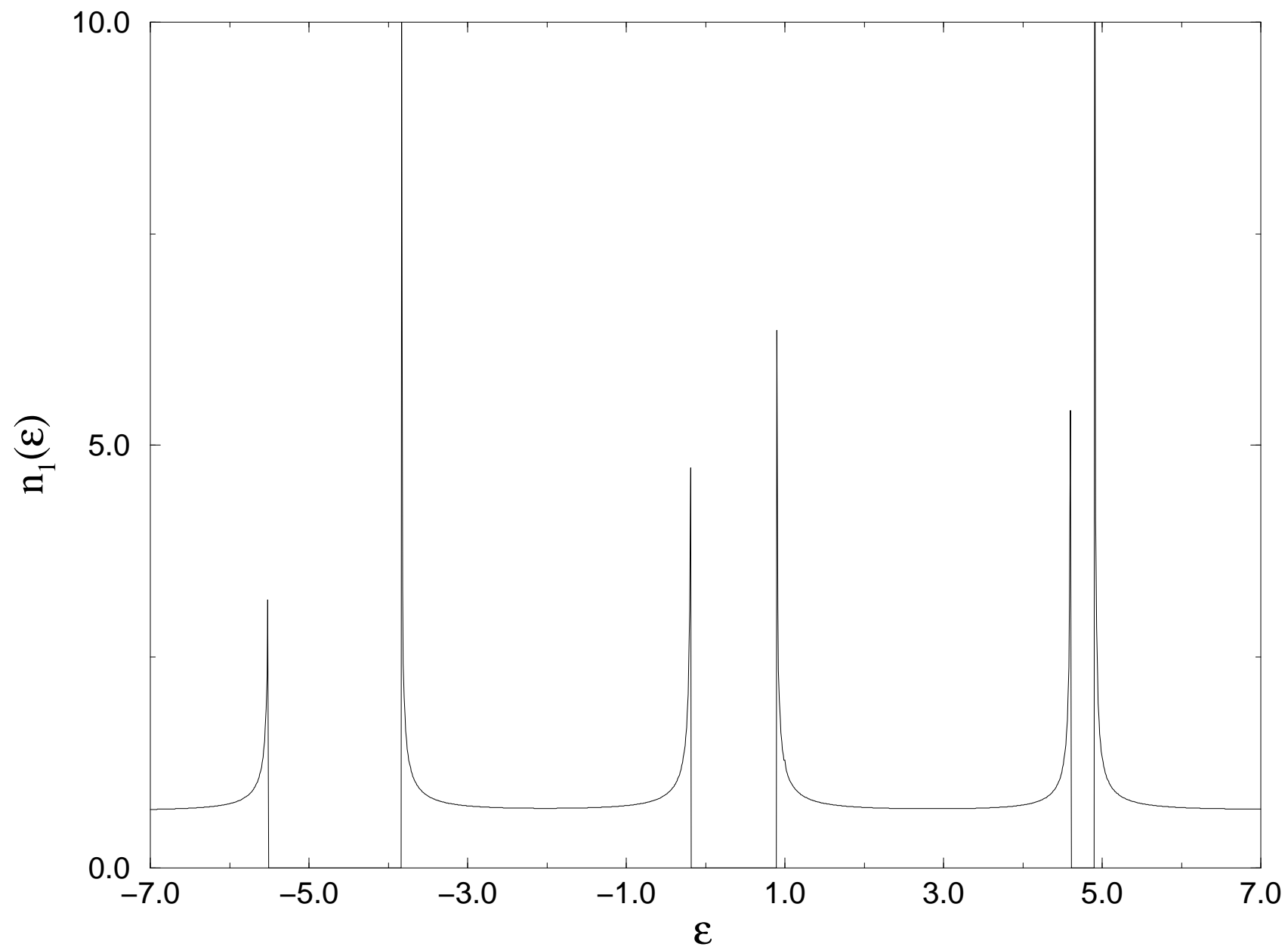


Fig.3(a)

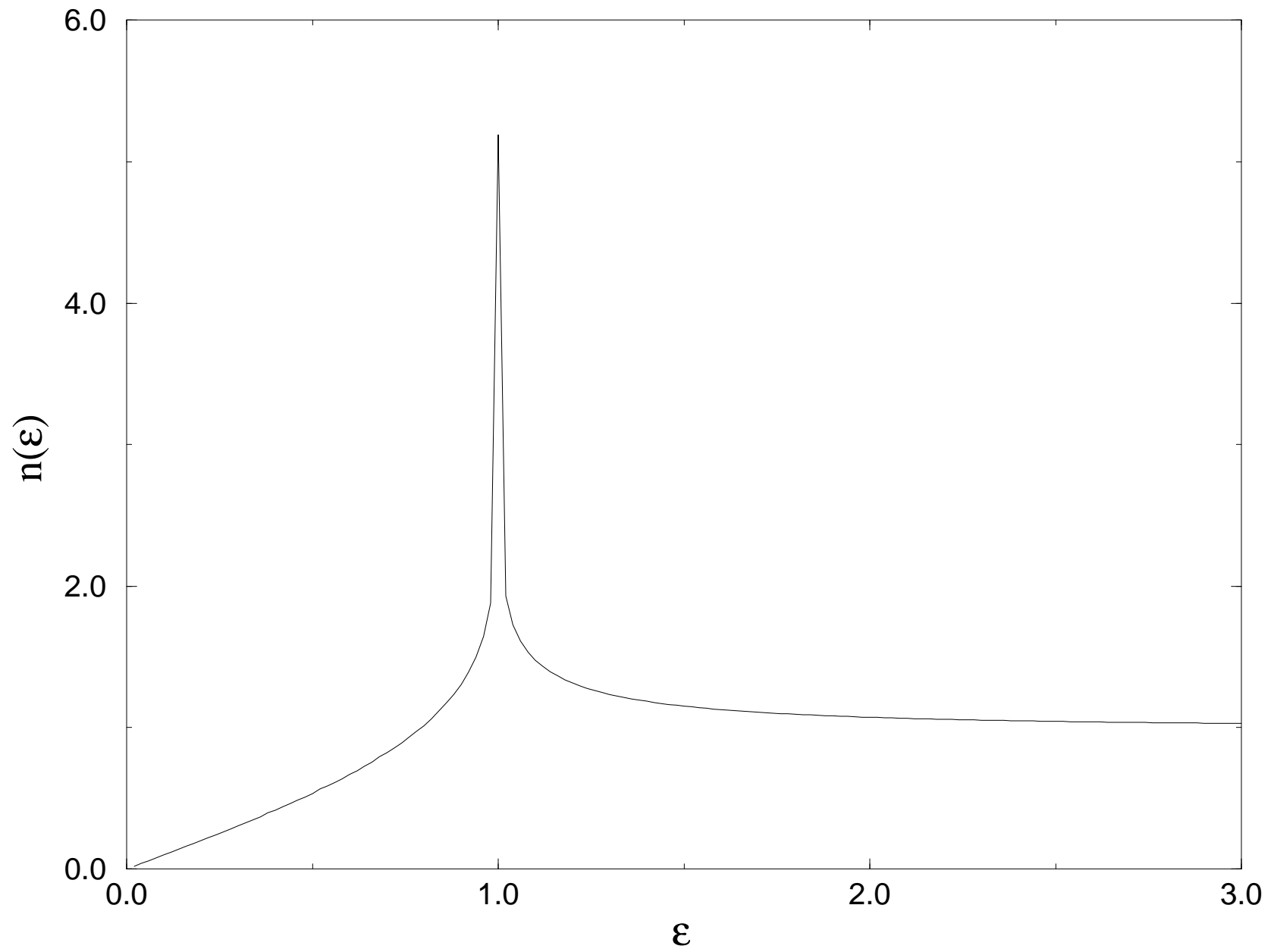


Fig. 3(b)

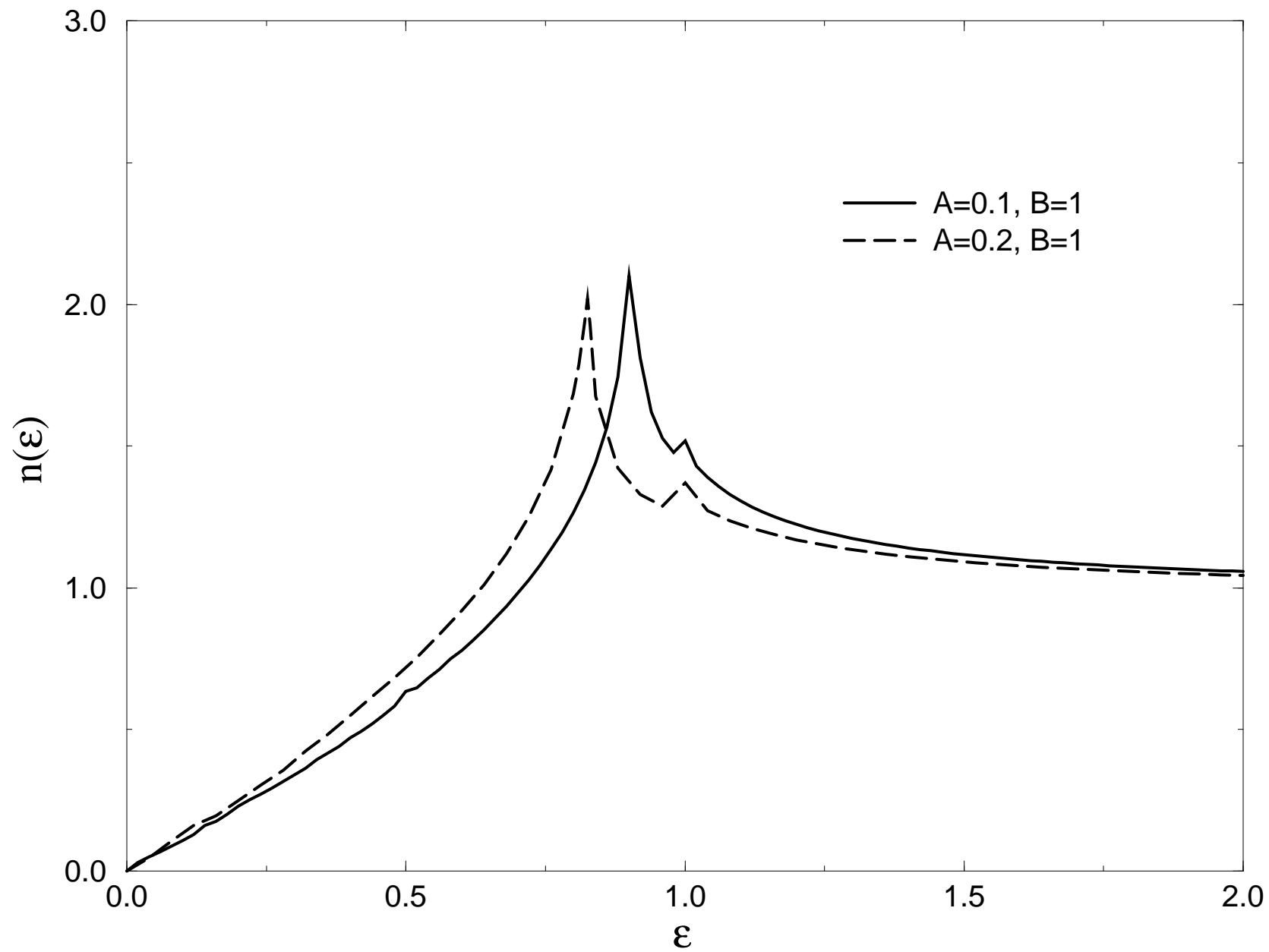


Fig. 3(c)

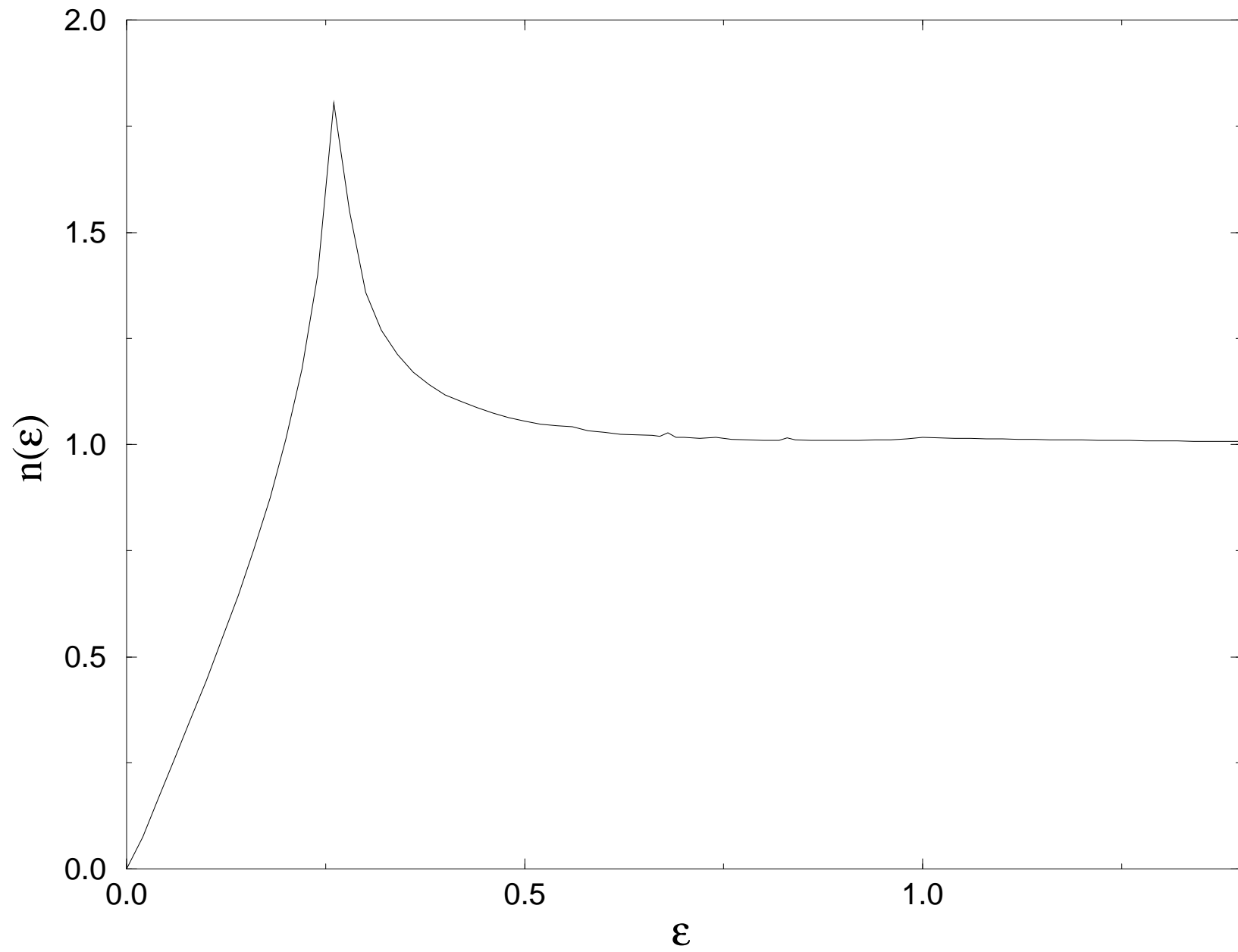


Fig. 4

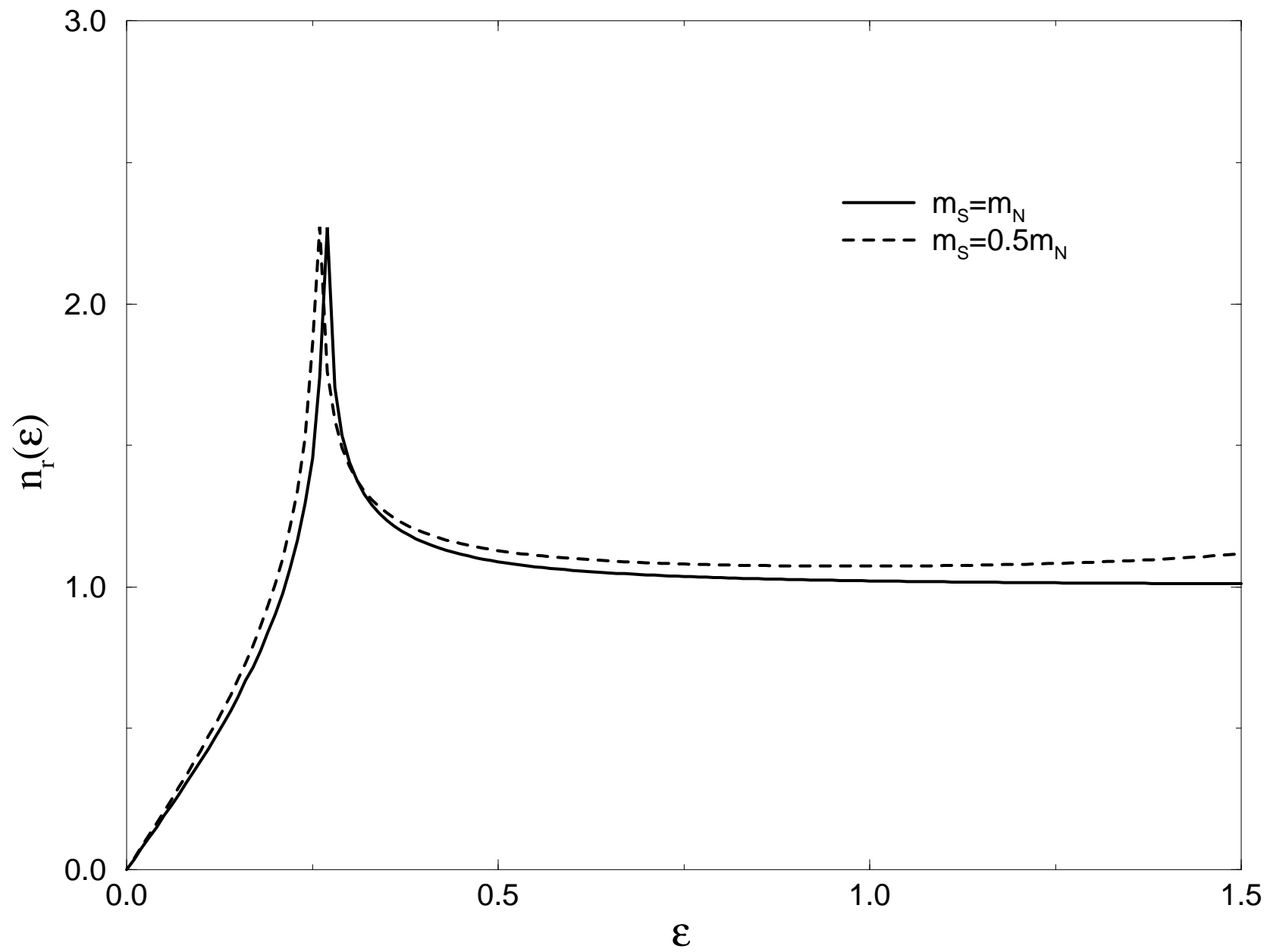


Fig. 5

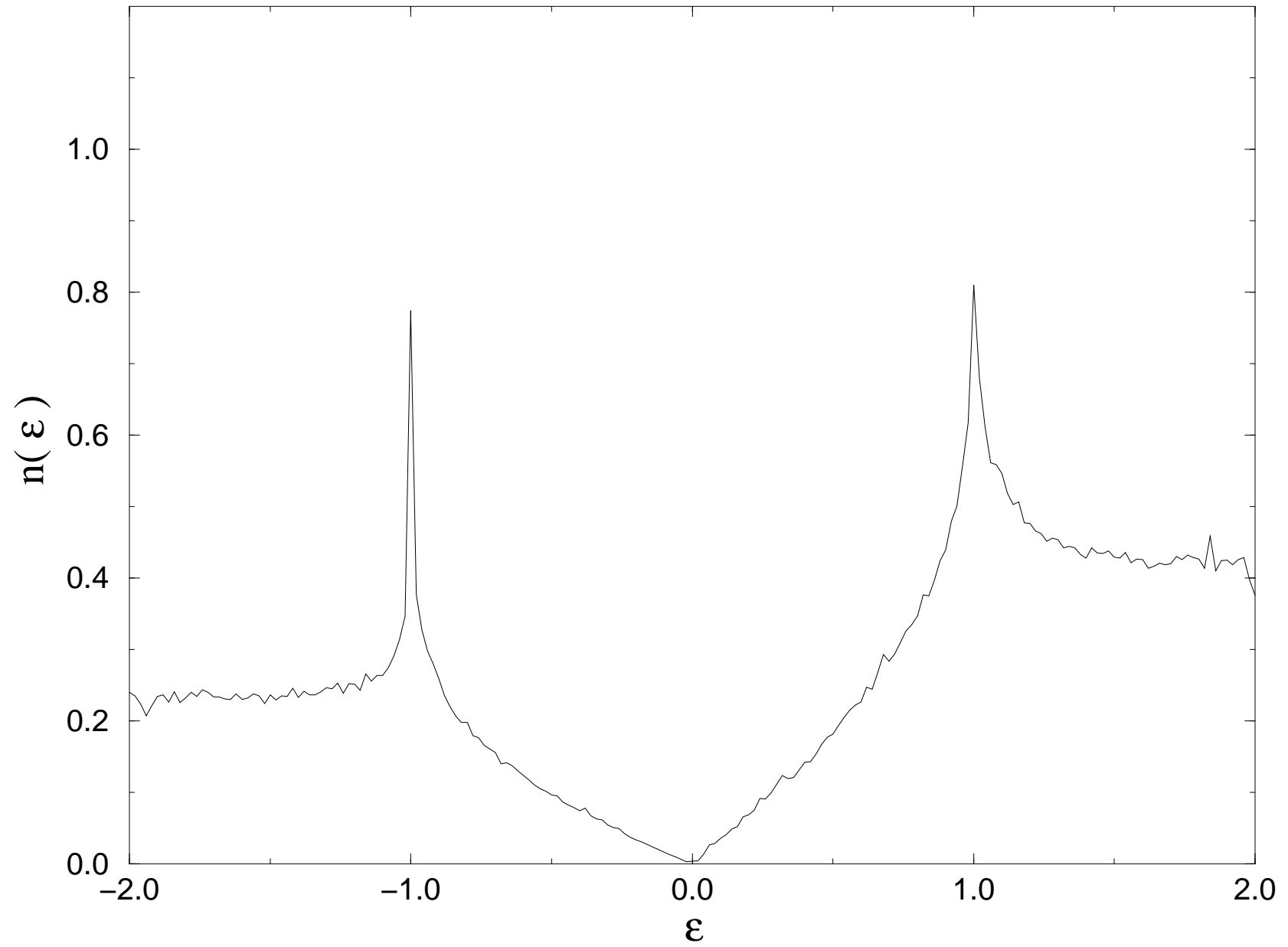


Fig.7(a)

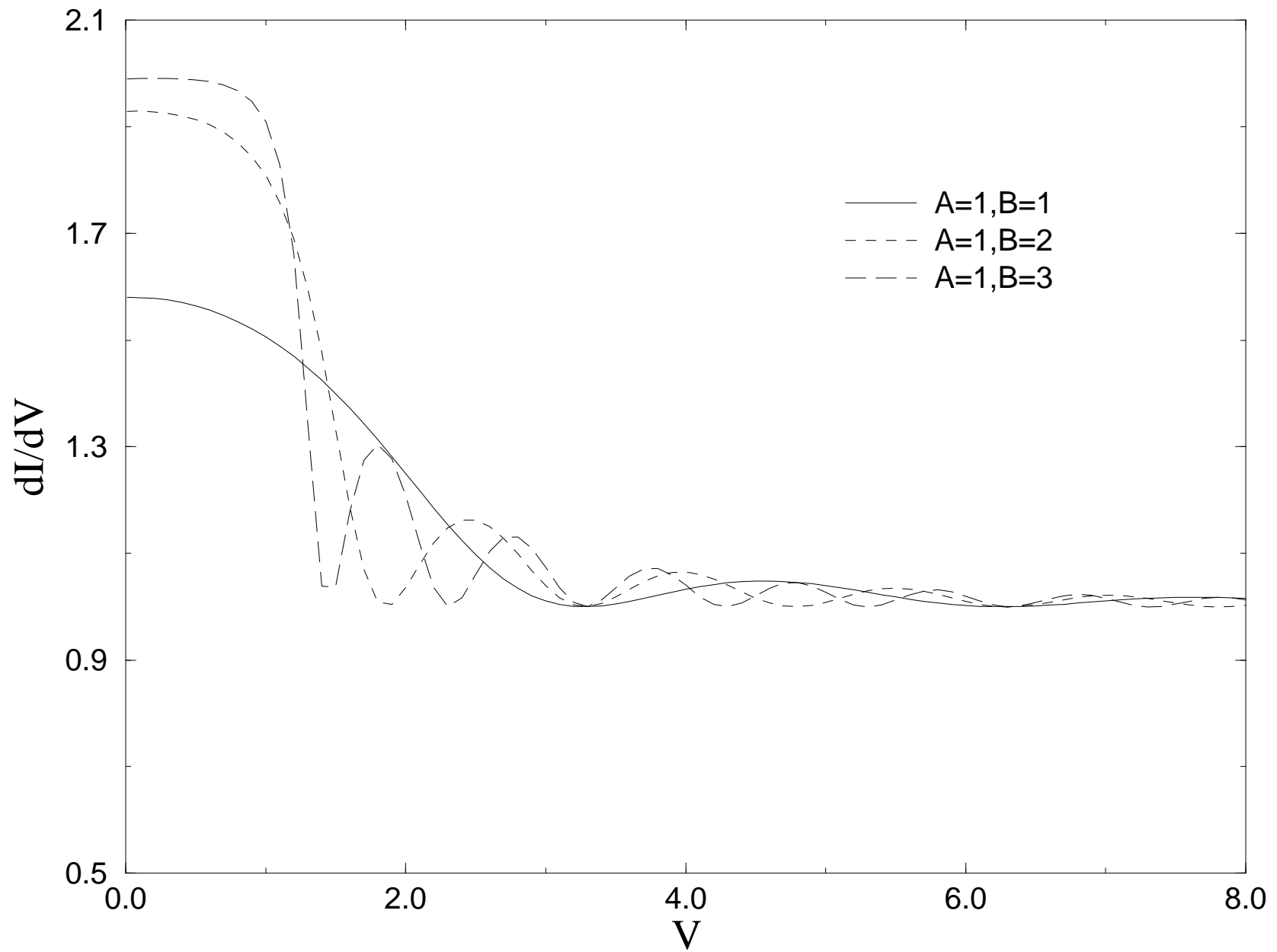


Fig. 7(b)

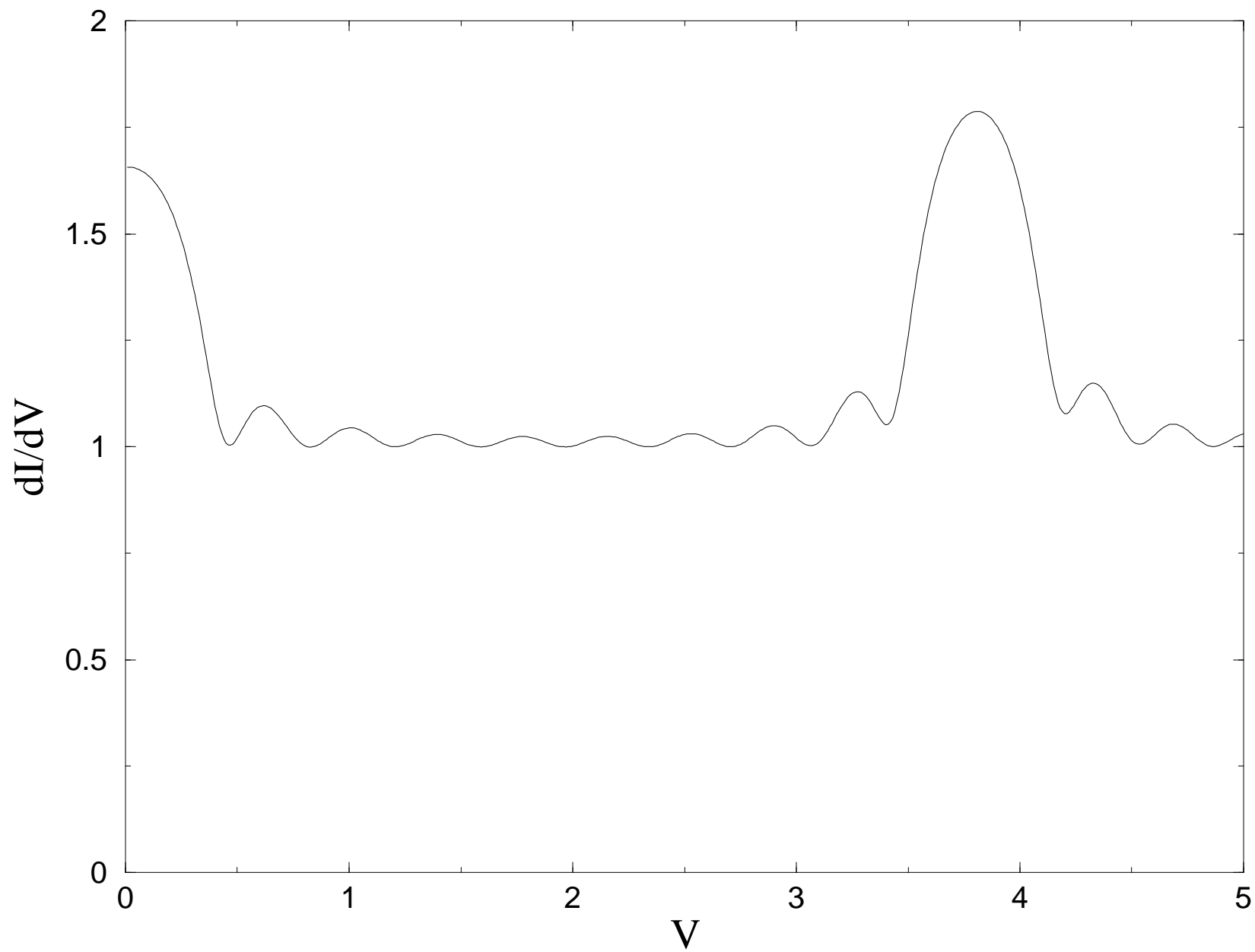


Fig.7(c)

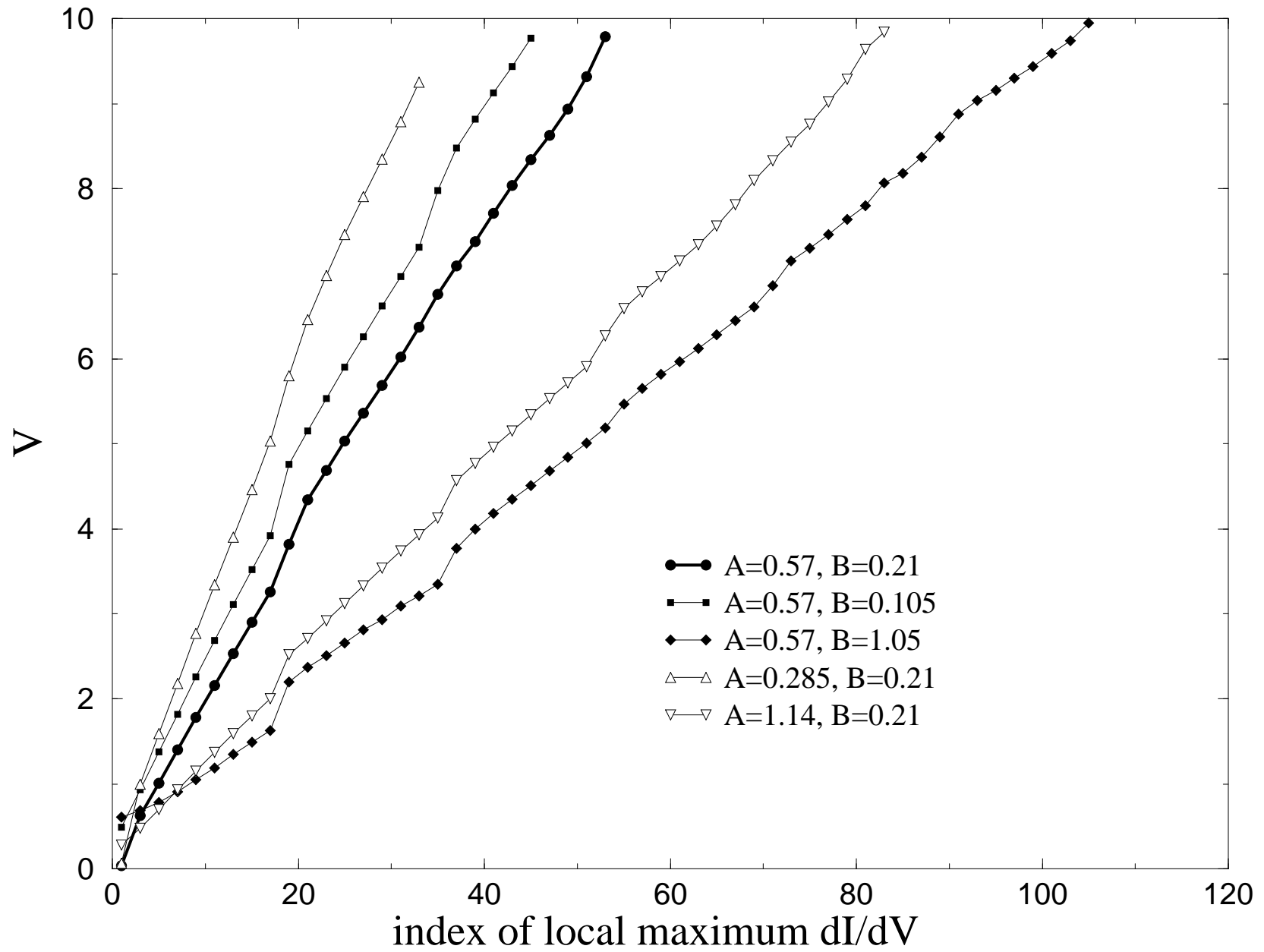


Fig. 7(d)

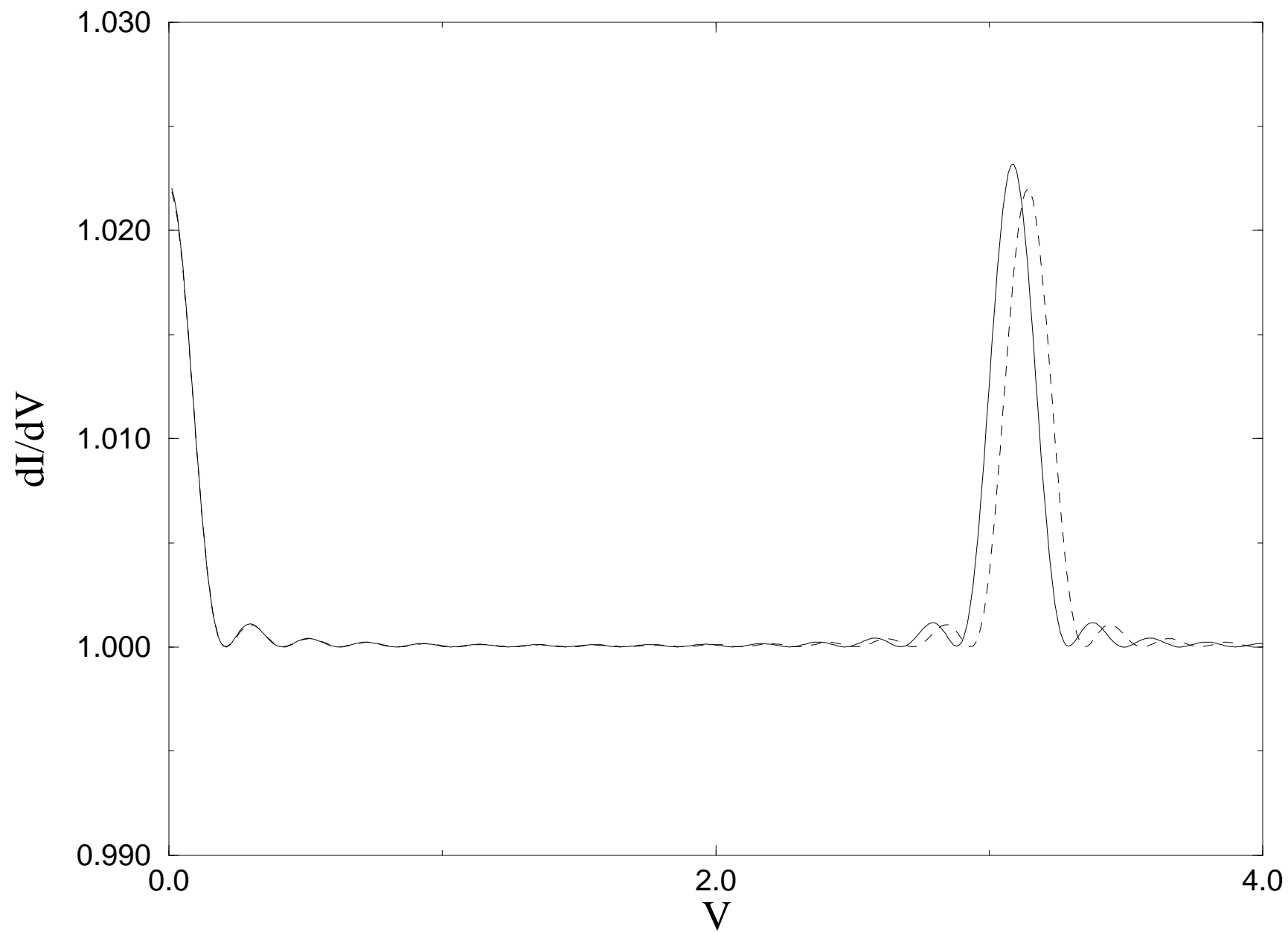


Fig.7(e)

